Energy & Environmental Science

PAPER

Cite this: *Energy Environ. Sci.*, 2016, **9**, 999

CO_2 conversion in a dielectric barrier discharge plasma: N_2 in the mix as a helping hand or problematic impurity?†

R. Snoeckx,*[a] S. Heijkers,[a] K. Van Wesenbeeck,[b] S. Lenaerts[b] and A. Bogaerts[a]

Received 29th October 2015,
Accepted 11th December 2015

DOI: 10.1039/c5ee03304g

www.rsc.org/ees

Carbon dioxide conversion and utilization has gained significant interest over the years. A novel gas conversion technique with great potential in this area is plasma technology. A lot of research has already been performed, but mostly on pure gases. In reality, N_2 will always be an important impurity in effluent gases. Therefore, we performed an extensive combined experimental and computational study on the effect of N_2 in the range of 1–98% on CO_2 splitting in dielectric barrier discharge (DBD) plasma. The presence of up to 50% N_2 in the mixture barely influences the effective (or overall) CO_2 conversion and energy efficiency, because the N_2 metastable molecules enhance the absolute CO_2 conversion, and this compensates for the lower CO_2 fraction in the mixture. Higher N_2 fractions, however, cause a drop in the CO_2 conversion and energy efficiency. Moreover, in the entire CO_2/N_2 mixing ratio, several harmful compounds, *i.e.*, N_2O and NO_x compounds, are produced in the range of several 100 ppm. The reaction pathways for the formation of these compounds are explained based on a kinetic analysis, which allows proposing solutions on how to prevent the formation of these harmful compounds.

Broader context

Environmental and energy applications of low temperature plasmas are worldwide gaining increasing interest. The central research question is whether plasma-based solutions can yield a valuable alternative to existing thermal processes. Nowadays, the conversion of CO_2 into chemicals and fuels is a hot topic. The worldwide transition to renewable energy gives plasma processes a clean electricity source, and due to their high operation flexibility, plasmas are very suitable for storing this intermittent sustainable energy in chemicals/fuels. Up to now most research is based on pure gases, however, in reality N_2 will be an important impurity. This is crucial, since its presence influences the plasma properties as well as the chemical pathways and thus the chemicals formed, for example, NO_x, which have detrimental effects on air quality and human health. This paper provides the necessary understanding by combining computations and experiments. The influence of N_2 on the CO_2 conversion as well as the NO_x production pathways are revealed for the first time, and the observed trends are explained, based on a kinetic analysis of the reaction chemistry. This approach allows us to look further down the road and go after solutions for the encountered problems regarding *e.g.* the unwanted NO_x formation.

Introduction

The steadily rising atmospheric concentration of CO_2 over the past century has a growing detrimental effect on our climate and environment, and is a threat for our society in general.[1–4] This results in a booming interest for technologies which can convert CO_2 into value-added products like chemicals and fuels,[5,6] as they can effectively convert waste into new feedstock, following the cradle-to-cradle principle.[7]

Several alternative (non-conventional) technologies are being investigated, such as photochemical, electrochemical and thermochemical pathways, either with or without catalysts, and all their possible combinations.[8–14]

Another new technology considered to have great potential in recent years is based on (non-thermal) plasma.[15] Several options are being investigated, including both pure CO_2 splitting into CO and O_2,[16–29] as well as the reaction with other gases, like CH_4 (dry reforming of methane),[30–47] H_2[32,48,49] or H_2O,[32,50–53] aiming for the production of syngas and valuable oxygenates, such as methanol, formaldehyde and formic acid. Most research on plasma-based CO_2 conversion is performed with dielectric barrier discharges (DBD),[16–22,30–39,41–44] microwave (MW) plasmas[22–26,30–32,46,52]

[a] *Research Group PLASMANT, Department of Chemistry, University of Antwerp, Universiteitsplein 1, BE-2610 Antwerp, Belgium. E-mail: ramses.snoeckx@uantwerpen.be*
[b] *Research Group DuEL, Department of Bioscience Engineering, University of Antwerp, Antwerp, Belgium*

† Electronic supplementary information (ESI) available. See DOI: 10.1039/c5ee03304g

and gliding arc (GA) discharges,[27–31,47,54] with a main focus on improving the energy efficiency of the conversion, as well as the selectivity towards value-added chemicals, in combination with catalysis.[21,26,32,41–46,48,55–57] To date, the highest energy efficiencies have been achieved with the GA and MW set-up, with values up to 43%[28,29,58] for the GA and up to 90% for the MW plasma being reported.[23,58] The energy efficiency of a DBD is more limited (typically up to 10%),[16,30,33] but can be improved by inserting a packing inside the plasma,[21,44,59] and the latter also easily allows the integration of a catalyst, for the selective production of value-added chemicals.

However, most research studies focus on "clean" CO_2 gas flows, while in reality most industrial gas flows contain impurities, for which it is economically unfeasible to be further purified. In most cases nitrogen is the main impurity.[9] Therefore, it is of uttermost importance to study the effect of N_2 impurities on the plasma chemistry of CO_2 conversion. The questions that come to mind are: how do these impurities affect the CO_2 conversion and energy efficiency, and more importantly, which byproducts (useful or harmful compounds) would be formed. This allows us to find out whether pre-(N_2) or post-(denox) purification steps would be needed and which one is to be preferred. Furthermore, if N_2O and other NO_x compounds are produced, it is important to know whether high enough concentrations might be obtained, to be considered relevant for nitrogen fixation.[60]

To provide answers to these important questions, we have performed experiments, supported by chemical reaction simulations, to increase the general understanding of the underlying mechanisms and pathways. We focus on a DBD as it has a very simple design and operates at atmospheric pressure, which is beneficial for up-scaling for industrial applications.[16] Both the effect of N_2 as an impurity (1 to 10%) as well as the effect of N_2 as an admixture or as a dilutant (10 to 98%) were studied. To our knowledge, only a few papers have reported on the effect of N_2 on CO_2 conversion, and only for a GA[28] and MW plasma,[24,25] while no papers have addressed the second question, *i.e.*, which byproducts are formed in the mixture and what are their consequences.

Description of the experiments

Plasma reactor

The experiments are carried out in a coaxial DBD reactor. A stainless steel mesh (ground electrode) is wrapped over the outside of a quartz tube with an outer and inner diameter of 22 and 16.5 mm, respectively, while a stainless steel rod with an outer diameter of 13 mm is placed in the center of the quartz tube and used as a high voltage electrode. The length of the discharge region is 90 mm, with a discharge gap of 1.75 mm, resulting in a discharge volume of 7.4 cm^3. CO_2 and N_2 are used as feed gases with a total flow rate of 611 mL min^{-1}. The N_2 content is controlled using mass flow controllers (Bronkhorst), and varied between 0 and 98%, in steps of 1% (in the regions of 0–10% and 90–98% N_2), while steps of 10% are used in the region between 10 and 90% N_2. The DBD reactor is powered by an AC high-voltage power supply (AFS), providing a maximum peak-to-peak voltage of 40 kV and a variable frequency of 1–90 kHz. The total current is recorded by a Rogowski-type current monitor (Pearson 4100), while a high voltage probe is used to measure the applied voltage. Furthermore, to obtain the charge generated in the discharge, the voltage on the external capacitor (10 nF) is measured. Finally, all the electrical signals are sampled by a four-channel digital oscilloscope (Picotech PicoScope 64201) and the discharge power is obtained by a control system used to calculate the area of the Q-U Lissajous Figures.[16] The precise experimental conditions can be found in the ESI.†

Product analysis: molecular gases

The feed and product gases are analyzed using a three-channel compact-gas chromatograph (CGC) (Interscience), equipped with two thermal conductivity detectors (TCD) and a flame ionization detector (FID). The first TCD channel is equipped with a Molecular Sieve 5A column for the separation of the molecular gases O_2, CO and N_2, while the second TCD channel contains an Rt-Q-BOND column for the measurement of CO_2, C_2–C_4 hydrocarbons and nitrogen containing compounds. The FID is equipped with an Rtx-5 column for the measurement of C_1–C_{10} and nitrogen containing compounds.

The absolute conversion, X_{abs}, of CO_2 and N_2 is calculated from the peak areas measured under the gas chromatograms:

$$X_{abs,CO_2} = \frac{\text{moles of } CO_2 \text{ converted}}{\text{moles of } CO_2 \text{ without plasma}} = \frac{\text{moles of } CO_2 \text{ without plasma} - \text{moles of } CO_2 \text{ with plasma}}{\text{moles of } CO_2 \text{ without plasma}} \quad (1)$$

$$X_{abs,N_2} = \frac{\text{moles of } N_2 \text{ converted}}{\text{moles of } N_2 \text{ without plasma}} = \frac{\text{moles of } N_2 \text{ without plasma} - \text{moles of } N_2 \text{ with plasma}}{\text{moles of } N_2 \text{ without plasma}} \quad (2)$$

The effective conversion, X_{eff}, is obtained by multiplying the absolute conversion, X_{abs}, with the relative gas content:

$$X_{eff,CO_2} = X_{abs,CO_2} \cdot [CO_2]\ (\%) \quad (3)$$

$$X_{eff,N_2} = X_{abs,N_2} \cdot [N_2]\ (\%) \quad (4)$$

To calculate the energy efficiency of the CO_2 conversion, we define the specific energy input (SEI) in the plasma from the discharge power and the gas flow rate:

$$\text{SEI}\left(\text{J cm}^{-3}\right) = \text{SEI}\left(\text{kJ L}^{-1}\right) = \frac{\text{Power (kW)}}{\text{Flowrate (L min}^{-1})} \cdot 60\ \left(\text{s min}^{-1}\right) \quad (5)$$

Subsequently, the energy efficiency (η) is calculated as:

$$\eta\ (\%) = X_{eff,CO_2} \cdot \frac{\Delta H_R\ \left(\text{kJ mol}^{-1}\right)}{\text{SEI (kJ L}^{-1}) \cdot 24.5\ (\text{L mol}^{-1})} \times 100\% \quad (6)$$

Note that the value of 24.5 L mol^{-1} is calculated for 298 K and 1 atm. Furthermore, ΔH_R is the reaction enthalpy for CO_2 splitting ($CO_2 \rightarrow CO + \frac{1}{2}O_2$), *i.e.* 279.8 kJ mol^{-1} or 2.9 eV per molecule.

Gas expansion factor

The moles of CO_2 and N_2, written in eqn (1) and (2), are as mentioned above, obtained with gas chromatography by sampling a small volume of the gas stream. Subsequently, the concentrations are deduced from a calibration curve, which is obtained for a constant gas flow. However, in a DBD the number of molecules and thus the volumetric flux increases along the reactor, as CO_2 is gradually converted into CO and O_2 molecules. More specifically, two CO_2 molecules are split into three molecules (see eqn (7)), which increase the volume by 50%.

$$2CO_2 \rightarrow 2CO + O_2 \quad (7)$$

As will be shown in section ''Effect of N_2 on plasma splitting of CO_2'' below, N_2 is almost not converted and thus its contribution to the change in volume is minimal. However, it does act as a dilutant: when adding more N_2, the volume expansion due to CO_2 splitting becomes less pronounced, since the share of CO_2 in the total gas mixture decreases.

This so-called gas expansion effect is clearly not taken into account in the gas chromatography approach above, which up to now is used by almost all authors. However, depending on the gas mixture it can be quite significant, as stated by Pinhão *et al.*[61] Therefore, in the present paper, we have properly accounted for this effect, as explained in detail in the ESI.† When neglecting this effect, the N_2 conversion would be overestimated by an order of magnitude. This is the result of the very low conversion for N_2, as shown below. Pinhão *et al.*[61] also reported that the relative error, and thus the overestimation, indeed increases significantly for lower values of the conversion. The CO_2 conversion, on the other hand, would be overestimated by a factor 1.5 for pure CO_2, a factor 1.2 for a mixture with 50% CO_2 and a factor 1.04 in the case of 10% CO_2 in the mixture. Indeed, as mentioned above, the volume expansion becomes less pronounced when more N_2 is present in the mixture. It is thus clear that when studying the effect of different gas mixing ratios, as in the present paper, the gas expansion effect will vary, depending on the gas mixing ratio, which further complicates the situation, and stresses the importance of taking this effect properly into account. More details about the calculation of the gas expansion effect can be found in the ESI.†

Product analysis: N_2O and NO_x compounds

Gas chromatography is not a suitable technique to study the formation of O_3, N_2O and NO_x compounds (*i.e.*, NO, NO_2, N_2O_3 and N_2O_5). Therefore, we applied Fourier transform infrared spectroscopy (FTIR; Thermo Fischer Scientific, Waltham, MA). By inserting a 2 m IR gas cell in the FTIR spectrometer, we obtain an IR absorption spectrum showing all IR active vibrations. During the experiments, an FTIR resolution of 1 cm^{-1} is used, which results in a spectrum being taken every 15 s. For basic qualitative measurements, this technique provides nearly real-time information on gas phase production of the N-containing compounds.

Description of the model

0D chemical kinetics model

The model used in this work to explain the plasma chemistry is a zero-dimensional (0D) chemical kinetics model, called ZDPlaskin.[62] In this model, the time-evolution of the species densities is calculated by balance equations, taking into account the various production and loss terms by chemical reactions. Transport processes are not considered; hence, the species densities are assumed to be constant in the entire simulation volume. Although this means that the plasma is treated as a ''batch reactor'', we can convert this to represent a ''plug-flow reactor'', which is indeed close to the real situation, by translating the temporal behavior into a spatial behavior, as described below. The rate coefficients of the heavy particle reactions (*i.e.*, atoms, molecules, radicals, ions, and excited species) are assumed to be constant and adopted from the literature (see below), whereas the rate coefficients for the electron impact reactions are calculated with a Boltzmann solver, BOLSIG+,[63] which is integrated into ZDPlaskin. For a more detailed description of the model, we refer to the work of Pancheshnyi *et al.*[62]

Plasma chemistry included in the model

The chemistry set used in this model was recently developed and validated for a microwave discharge.[25] In short, it considers 119 different species (see Table 1), which react with each other in 339 electron impact reactions, 804 ion reactions and 2795 neutral reactions. Their corresponding rate coefficients, and the references where these data were adopted from, are listed in the ESI† of our previous work.[25] Some minor adjustments were made, which are explained in the ESI† of the current paper.

Table 1 Species included in the model, besides the electrons. The symbols 'V' and 'E' stand for various vibrational and electronically excited levels of the various species, as explained in detail in the work of Heijkers *et al.*[25]

Molecules	Radicals	Charged species	Excited species
CO_2	C_2O, C_2, C	CO_2^+, $C_2O_2^+$, $C_2O_3^+$, $C_2O_4^+$, C_2^+, C^+	CO_2(Va), CO_2(Vb), CO_2(Vc), CO_2(Vd), CO_2(V1–V21), CO_2(E1), CO_2(E2)
CO		CO^+, CO_3^-, CO_4^-, CO_4^+	CO(V1–V10), CO(E1), CO(E2), CO(E3), CO(E4)
O_2, O_3	O	O_2^+, O_2^-, O^+, O^-, O_4^-, O_4^+, O_3^-	O_2(V1), O_2(V2), O_2(V3), O_2(V4), O_2(E1), O_2(E2)
N_2	N	N^+, N_2^+, N_3^+, N_4^+	N_2(V1–V14), $N_2(C^3\Pi_u)$, $N_2(A^3\Sigma_u^+)$, $N_2(a'^1\Sigma_u^-)$, $N_2(B^3\Pi_g)$, N(2D), N(2P)
N_2O, N_2O_3, N_2O_4, N_2O_5	NO, NO_2, NO_3	NO^+, N_2O^+, NO_2^+, NO^-, N_2O^-, NO_2^-, NO_3^-, $N_2O_2^+$	
ONCN, C_2N_2, NCN	CN, NCO		

Application of the 0D model to a DBD reactor

As mentioned above, a 0D model calculates the species densities as a function of time only, and it neglects spatial variations. However, the time evolution can be translated into a spatial evolution (*i.e.* as a function of position in the DBD reactor) by means of the gas flow rate. This allows us to mimic the typical filamentary behavior of a DBD used for CO_2 conversion.[16,64] Indeed, the gas molecules will pass through several micro-discharge filaments on their way throughout the reactor. This is thus taken into account in the model by applying a large number of consecutive microdischarge pulses of 30 ns, in exactly the same way as described by Kozák *et al.*[22] This approach has already proven to be applicable for a variety of conditions and gas mixtures.[18,20,22,33,35,65,66] We assume the same gas flow rate as used experimentally, *i.e.*, 611 mL min^{-1} at atmospheric pressure, and the same DBD reactor volume of 7.4 cm^3 (see Section "Plasma reactor" above), which corresponds to a total residence time of 0.73 s. The temperature is assumed to remain constant at 300 K, as predicted by Aerts *et al.*[16]

Results and discussion

First, we will show the experimental results and compare them with the model predictions, for the conversion of CO_2 and N_2, the energy efficiency of CO_2 conversion and the formation of N_2O and NO_x compounds, upon addition of N_2 in the gas mixture. Subsequently, the underlying plasma chemistry for the CO_2 and N_2 conversion and the formation of the various compounds will be discussed in more detail, based on the modeling results.

Effect of N_2 on plasma splitting of CO_2

Effect on conversion and energy efficiency. Fig. 1(a) illustrates the experimental and calculated absolute CO_2 and N_2 conversion as a function of the N_2 content. The absolute CO_2 conversion increases more or less exponentially with rising N_2 fraction, both in the experimental data and the calculations. This indicates that N_2 has a beneficial effect on CO_2 splitting, as will be explained below. The N_2 conversion, on the other hand, is very low, *i.e.*, in the order of 0.1–1% for both the experiments and the model, showing again a good agreement. The reason for the low N_2 conversion is that it mainly occurs through electron impact ionization of N_2 molecules, followed by the reaction of the produced ions with other species, as we explained before for a CH_4/N_2 mixture.[65] However, this electron impact ionization occurs at high electron energy (above 15.5 eV), which is higher than the values typically reached for our operating conditions, and this explains the low N_2 conversion.

Fig. 1(b) illustrates the experimental and calculated effective (or overall) CO_2 and N_2 conversion as a function of the N_2 content. The effective CO_2 conversion remains relatively constant at around 4% when adding up to 40–50% N_2. This can be explained because the absolute conversion increases (*cf.* Fig. 1(a)), but at the same time the fraction of CO_2 in the gas mixture decreases, and both effects compensate each other. In other words, the increase in absolute conversion upon adding N_2 is high enough to counteract the lower CO_2 concentration in the gas mixture. When reaching 50% N_2, the effective conversion starts decreasing exponentially. This means that the increase in absolute conversion is no longer high enough to compensate for the lower CO_2 concentration in the mixture. This behavior can be explained from the kinetic analysis presented in section "Underlying chemistry" below. When adding up to 50% N_2, the energy put into the plasma goes to CO_2 splitting, both directly through electron impact dissociation and indirectly through

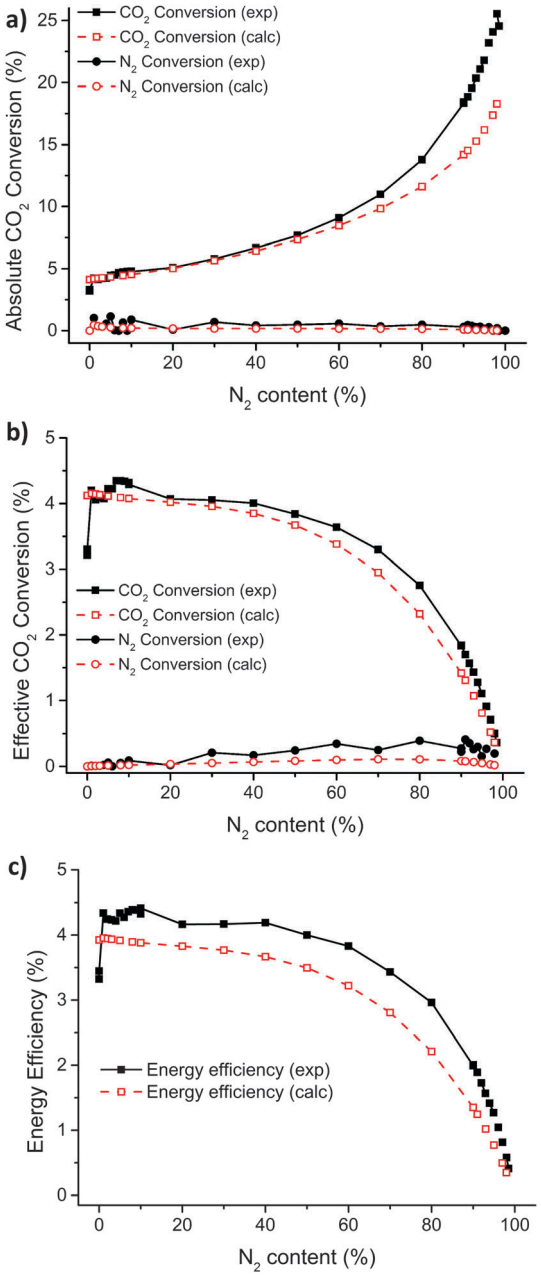

Fig. 1 Experimental and calculated values of absolute CO_2 and N_2 conversion (a), effective CO_2 and N_2 conversion (b) and energy efficiency of CO_2 conversion (c) as a function of N_2 content, for a residence time of 0.73 s and a SEI of approx. 12 J cm^{-3}.

electron impact excitation of N_2, which aids in the dissociation of CO_2 (see below). Above 50% N_2, more energy goes into N_2 excitations and it is no longer efficiently transferred to the reactions leading to CO_2 dissociation (see section "Underlying chemistry" below).

Again, excellent agreement is obtained between the experimental and calculated data, except in the region between 0 and 1% N_2, where a significant rise in CO_2 conversion is seen in the experiments, being absent in the model predictions. This is attributed to a change in the physical properties of the discharge when comparing a pure CO_2 plasma with a CO_2/N_2 plasma. Indeed, it is known that a DBD plasma in CO_2 has a filamentary character,[16,64] while adding N_2 leads to a more homogeneous and stable discharge.[65,67] This effect cannot be completely captured in the 0D model, explaining the slight discrepancy between experiments and model predictions.

The effective N_2 conversion rises slightly (from 0.01 to 0.3% in the experiment, and from 0.005 to 0.1% in the model predictions) when adding up to 90% N_2, followed by a drop to zero for pure N_2. This behavior can again be explained by the fact that the N_2 conversion occurs through ionization and the subsequent reaction of the formed ions with other species (see above), which are absent for pure N_2. The small difference in experimental and calculated values comes from the large uncertainties in the experiment, resulting from the low values and thus the large effect of the gas expansion factor, as discussed in the Experimental section above.

The energy efficiency for CO_2 conversion (see Fig. 1(c)) shows exactly the same trend as the effective CO_2 conversion, where it is calculated from (see eqn (6) above). Thus, the energy efficiency remains quite constant around 4% in the experiments (and slightly lower in the model predictions) until about 50% N_2 and then it starts decreasing rapidly, because of the lower effective CO_2 conversion and the fact that more energy is consumed by the N_2 molecules upon increasing N_2 content in the mixture, and cannot be used anymore for the CO_2 conversion.

Effect on product formation. CO_2 splitting typically yields CO and O_2 molecules; the latter being formed by the recombination of O atoms. Besides, also some O_3 can be created.[18] This product distribution does not change when adding N_2, as revealed by our experiments and model predictions. However, the N_2 addition leads to the formation of some N_2O and NO_x compounds, which will be discussed in more detail in this section. This is very important because the production of N_2O and certain NO_x might be beneficial when formed in very high concentrations, as this would indicate that the process could be effective for nitrogen fixation.[60] However, in low concentrations (*i.e.*, below 1%), it has no economic value, and even worse, it gives a high environmental cost, since N_2O and NO_x have a severe negative impact on air quality, leading to restriction of their emissions and the need of denox installations.[68,69] Therefore, it is of crucial importance to analyze the product formation in the CO_2/N_2 plasma, to know which of the two scenarios take place.

For NO and NO_2 a calibration curve is available, which allows us to express the measurement results in absolute concentrations (ppm). For N_2O, N_2O_3 and N_2O_5, however, this is not the case and the formation of these compounds can thus only be expressed in arbitrary units (a.u.) of the measured absorbance. To maintain consistency throughout the discussion here, all experimental results will be presented in arbitrary units (a.u.) as measured absorbance with the FTIR-cell, while the calculation results will be given in ppm. For NO and NO_2, we will elaborate on the comparison in absolute concentrations in the ESI,† and briefly report about it in the text below. Furthermore, to allow a detailed comparison between the experimental and calculated trends, the two *y*-axes (representing the experimental and calculated data, respectively) will be constructed so that they vary over the same range.

The measured and calculated NO and NO_2 concentrations are plotted as a function of N_2 content in the gas mixture in Fig. 2(a) and (b), respectively. Experimentally both compounds follow the same parabolic trend with a maximum at 50% N_2. As will be illustrated in section "N_2O and NO_x formation" below, the NO_x species are formed out of N (or $N_2(A^3\Sigma_u^+)$) and O atoms, which originate from N_2 and CO_2, respectively. Thus, it is not unexpected that the maximum of the NO_x concentration is achieved when both reactants are present in approximately equal concentrations. The calculated results follow more or less the same trend for NO_2 but a left-skewed trend for NO with respect to the experimental values. Nevertheless, in both cases, the profiles first rise and then drop with increasing N_2 content, so we believe that the model can be used to explain the observed trends (see section "N_2O and NO_x formation" below).

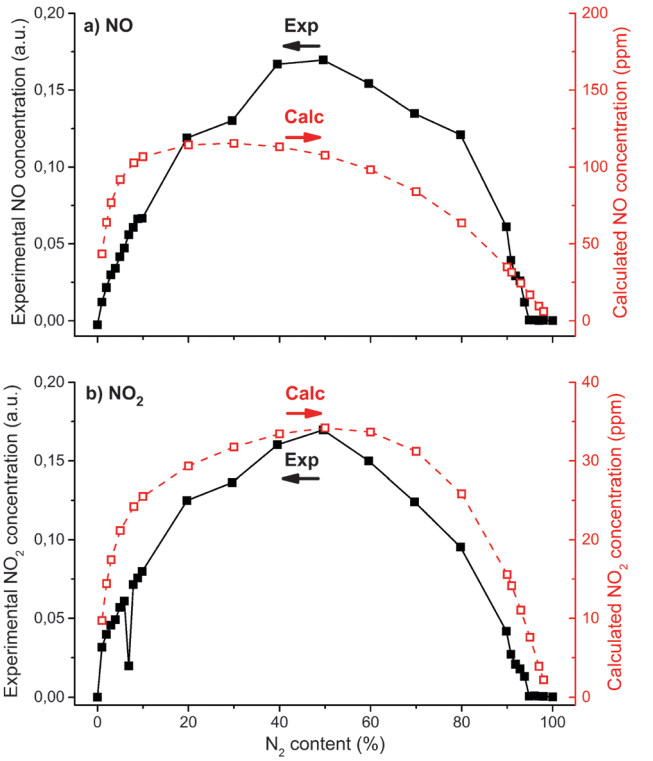

Fig. 2 Experimental and calculated concentrations of NO (a) and NO_2 (b) as a function of N_2 content, for a residence time of 0.73 s and a SEI of approx. 12 J cm^{-3}.

Furthermore, even the absolute values of the concentrations are in reasonable agreement, as elaborated in the ESI.†

Experimentally, the obtained NO concentration is about an order of magnitude higher than the NO_2 concentration, with maximum values of 550 and 54 ppm, respectively (see ESI†). Even at 1% N_2 the measured concentrations are already 40 and 10 ppm, respectively. To put these values in perspective, when converting them to emissions in the common units of g km^{-1} in the automobile sector,[70] they are ~3000 times higher than that currently allowed under European emission standards for passenger cars (EURO 6 norm, 80 mg km^{-1}).[71] Compared with industrial emissions, when converting them to the industrially used units of mg m^{-3}, they are in the order of 10–20 times higher than the current BAT-AELs (Best Available Technique Associated Emission Levels) for coal fired power plants with a capacity of >300 MW in Europe, which allow NO_x emissions of 50–200 mg m^{-3}.[72] The calculated NO and NO_2 concentrations are somewhat lower, but in the same order of magnitude, with a maximum of 115 and 34 ppm, respectively.

These NO_x compounds react in the air, resulting in smog formation and acid rain. Thus, these high concentrations will have a negative effect on air quality and the environment.[73] At the same time, however, the concentrations are too low to be considered useful for nitrogen fixation.[60] Indeed, the current industrial processes for nitrogen fixation, *i.e.*, the Haber–Bosch process (for making ammonia) and the Ostwald process (for making nitric acid starting from ammonia) can achieve overall yields of 99%.[74]

The other NO_x compounds detected in the experiments are N_2O_3 and N_2O_5, for which the concentrations (again in a.u.) are plotted in Fig. 3(a) and (b), along with the model predictions (in ppm). Again, a reasonable agreement is obtained in the experimental and calculated trends, especially for N_2O_5 (note the same variation in the orders of magnitude of both *y*-axes).

The N_2O_3 and N_2O_5 concentrations vary over two and three orders of magnitude, respectively, within the entire range of N_2 contents in the gas mixture. According to our calculations, concentrations up to 1000 ppm are found for N_2O_5, while the calculated N_2O_3 concentrations do not exceed 0.05 ppm. Unfortunately, we were not able to deduce the absolute values for the experimental concentrations, because of lack of suitable detectors to create a calibration curve. Since N_2O_5 can be considered as the anhydride of nitric acid, this would indicate that if the calculated concentrations are realistic, these concentrations would contribute heavily to the formation of acid rain if emitted to the atmosphere. Regarding the N_2O_3 emission, this appears not to be a problem, since the calculations predict negligible amounts to be formed. This is in agreement with the fact that at room temperature the dissociation into the constituent gases NO and NO_2 is favored over the formation of N_2O_3.[75]

Finally, the measured and calculated N_2O concentrations are presented in Fig. 4. Again the same parabolic trend as a function of the N_2 content in the gas mixture is observed as for the NO_x compounds, with a maximum at 50–60% N_2. The calculated maximum concentration is about 55 ppm, but experimentally it was again not possible to obtain absolute values of

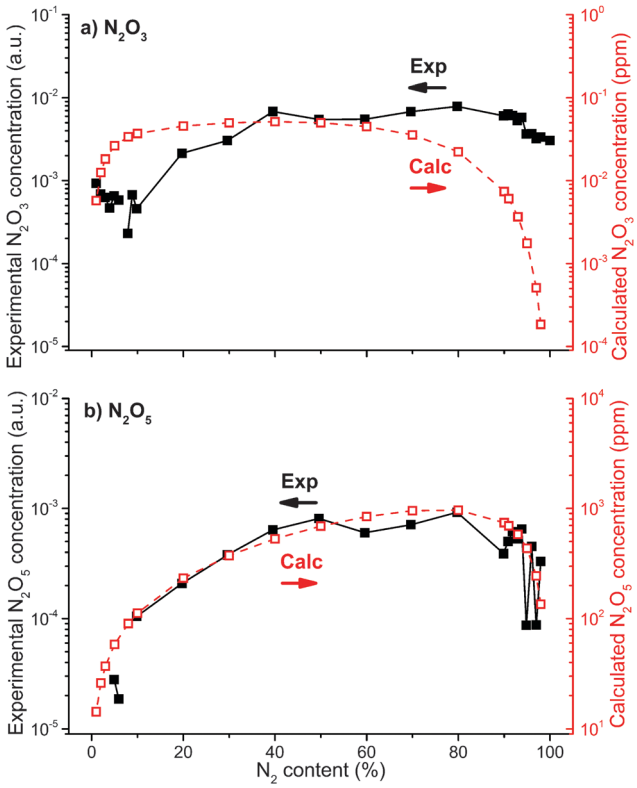

Fig. 3 Experimental and calculated concentrations of N_2O_3 (a) and N_2O_5 (b) as a function of N_2 content, for a residence time of 0.73 s and a SEI of approx. 12 J cm^{-3}.

the concentration. Nitrous oxide is a very potent greenhouse gas, with a global warming potential (GWP) of 298 $CO_{2,equivalent}$. Keeping in mind that for the conditions under study, we effectively convert about 4% CO_2 (see Fig. 1(b) above), this means that if the N_2O concentration would exceed 130 ppm, the reduction in GWP would be equal to zero. Hence, the production of nitrous oxide is voiding the greenhouse gas mitigation potential of our technology (by up to 40% for N_2O concentrations up to 55 ppm) if we do not add a denox purification step

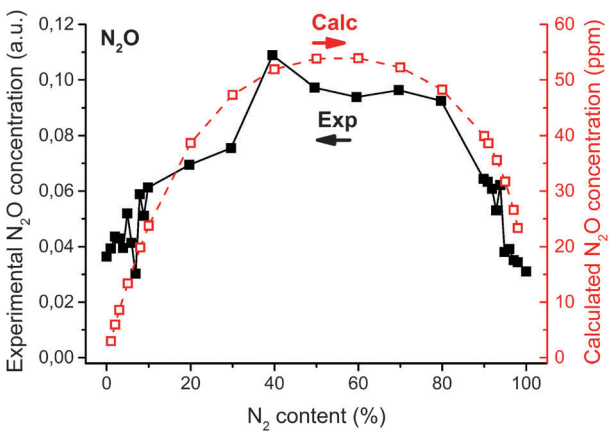

Fig. 4 Experimental and calculated concentrations of N_2O as a function of N_2 content, for a residence time of 0.73 s and a SEI of approx. 12 J cm^{-3}.

afterwards. Denox technology mainly includes Selective non-Catalytic Reduction (SNCR), Selective Catalytic Reduction (SCR) and a combination of both. Although these are already mature technologies with high NO_x reduction efficiencies (70–95%), they are also prone to high operational costs.[76,77] This is no surprise since in general, end-of-pipe clean-up technology is always more expensive.

It becomes clear from both the measurements and the calculations that N_2O and several NO_x compounds are produced. Although their concentrations remain in the ppm range, this is certainly not negligible, since they give rise to several environmental problems. Hence, it appears to be crucial to separate the CO_2 gas from N_2 impurities (or gas fractions) before plasma treatment, to avoid the formation of NO_x compounds and thus the need to install expensive denox installations afterwards.

Underlying chemistry

In the following sections, the underlying plasma chemistry, as predicted by the model, will be discussed in more detail, for the CO_2 conversion in the presence of N_2, as well as for the formation of NO_x compounds and N_2O. Indeed, a better insight into the underlying chemical reactions might help to steer the process, to improve the CO_2 conversion and energy efficiency, and to reduce the NO_x and N_2O formation.

CO_2 conversion. The reactions responsible for the CO_2 conversion are presented in Fig. 5, as a function of the N_2 content in the gas mixture. At low N_2 contents, the most important reaction is electron impact dissociation of CO_2 into CO and O, while at high N_2 contents, the reaction with metastable $N_2(A^3\Sigma_u^+)$ molecules, yielding the same splitting products (CO and O) and leaving N_2 in its ground state, is mainly responsible for the CO_2 conversion. Indeed, upon higher N_2 contents, the electron energy is gradually being used for N_2 excitation instead of CO_2 dissociation, explaining the drop in electron impact dissociation rate and the corresponding increase in the dissociation rate by N_2 metastable molecules. The former reaction is dominant during the microdischarge filaments of the DBD, as is illustrated in the ESI,† while the latter reaction is more important in the time between the filaments, *i.e.*, the so-called afterglows. Other reactions that play a minor role towards CO_2 dissociation (~5%) are electron impact ionization of CO_2 and electron impact dissociation from vibrationally excited CO_2 (*i.e.*, $CO_2(V)$) (see Fig. 5).

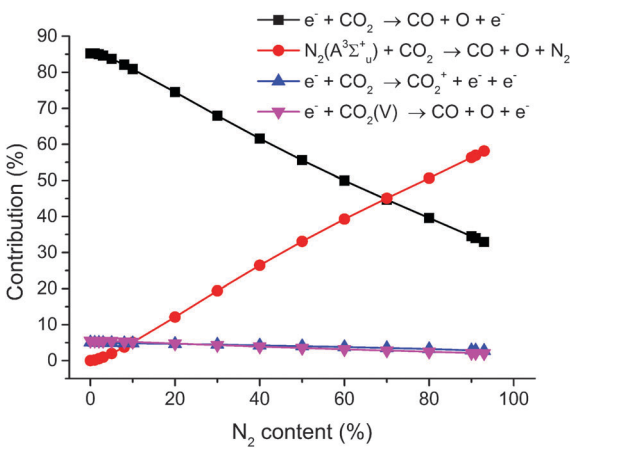

Fig. 5 Relative contribution of the main processes leading to CO_2 conversion as a function of N_2 content, for a residence time of 0.73 s and a SEI of approx. 12 J cm^{-3}.

Up to 60–70% N_2, the sum of the rates due to electron impact dissociation and dissociation by N_2 metastable molecules drops only slightly upon increasing N_2 content, explaining why the effective CO_2 conversion drops only slightly, as shown in Fig. 1(b). In other words, upon adding N_2, the N_2 metastable molecules provide an extra dissociation mechanism for CO_2, explaining why the absolute CO_2 conversion rises (Fig. 1(a)), but this is compensated by the lower CO_2 content in the mixture, leading to a slight drop in effective CO_2 conversion. Above 70% N_2, however, both rates start decreasing due to the lower CO_2 concentration, which is not compensated by the higher N_2 concentration (and thus higher dissociation by N_2 metastable molecules), leading to a drop in the effective CO_2 conversion.

N_2O and NO_x formation. The most important formation and destruction processes for NO, NO_2 and N_2O are presented in Fig. 6, 7 and 8, respectively. Our calculations predict that NO is mainly formed during the afterglows, *i.e.*, in between the microdischarge filaments, because it is dictated by heavy particle reactions (see ESI†). The dominant formation mechanism of NO is the reaction between O radicals and NO_2 molecules, forming NO and O_2 molecules.

This reaction is by far the most important for N_2 fractions below 95% (see Fig. 6(a)). Above 95%, the reaction between N radicals and ozone, yielding the same products, becomes slightly more important.

The dominant NO loss mechanism is the recombination with O atoms into NO_2 through a three-body reaction. This third body can be either CO_2 (mainly important for N_2 contents below 40%) or N_2 (for N_2 contents between 40 and 90%). For N_2 contents above 95% the reaction with N atoms, yielding the formation of O and N_2, becomes most important. Other loss mechanisms are the formation of N_2O_3 (mainly at N_2 fractions below 70%) and the reaction with electronically excited $N_2(a'^1\Sigma_u^-)$, forming N_2, N and O (at higher N_2 fractions). However, these reactions do not contribute to more than ~5–20%.

It is thus clear that there is an interplay between NO and NO_2, as was also observed in other modeling work, albeit for other conditions (*i.e.*, a plasma jet expanding in humid air).[78] NO_2 is the main source of NO production and *vice versa*, as will be shown in Fig. 7. This will also become clear from the reaction scheme in Fig. 9 below.

The NO_2 production also occurs mainly in between the filaments, attributed to heavy particle reactions. The only important process for NO_2 production is the three-body recombination between NO and O, with either CO_2 or N_2 as a third body (at N_2 contents below and above 40%, respectively; see Fig. 7(a)). These are also the main loss mechanisms of NO, as is illustrated in Fig. 6(b). Some other processes, like the dissociation of N_2O_3 into NO and NO_2, the reaction between NO_3 and NO, forming two NO_2 molecules, or between NO_3 and O, forming NO_2 and O_2, also play a minor role (~5–20%) in the production of NO_2.

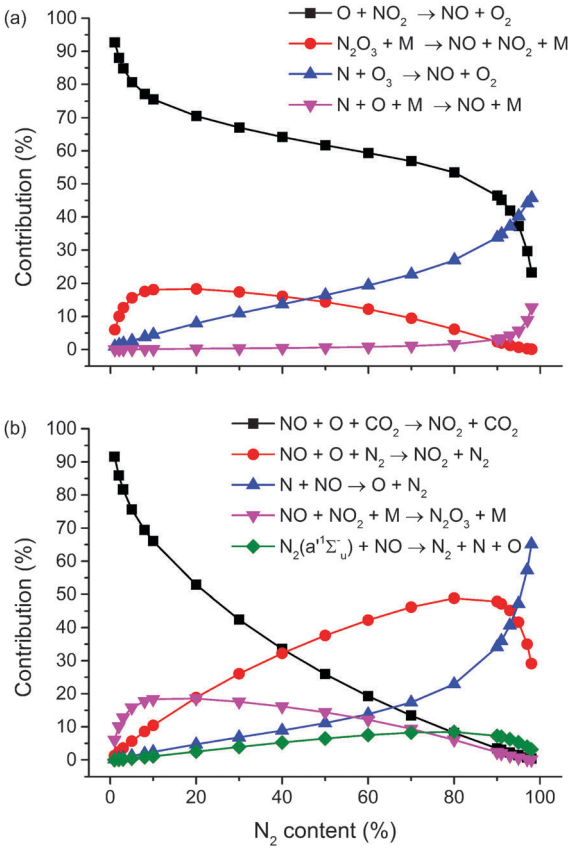

Fig. 6 Relative contributions of the main formation (a) and loss (b) mechanisms of NO as a function of N_2 content, for a residence time of 0.73 s and a SEI of approx. 12 J cm^{-3}.

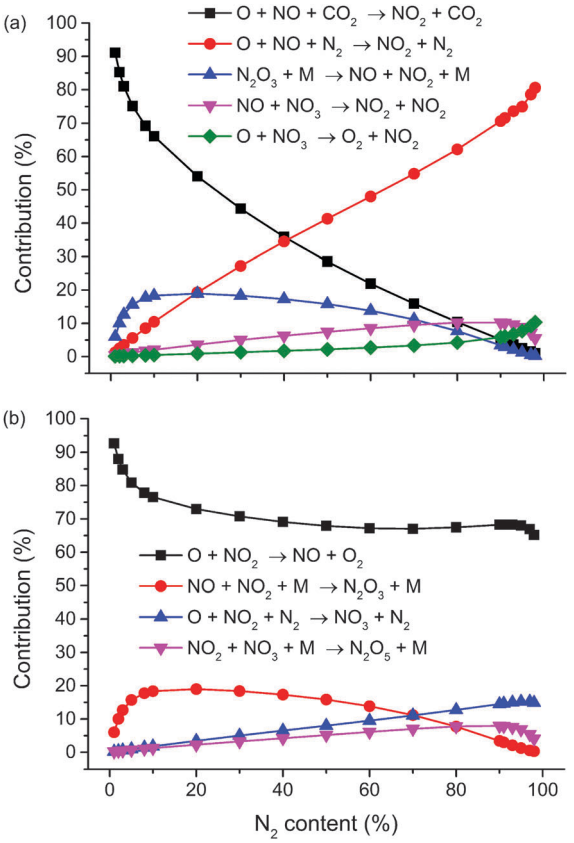

Fig. 7 Relative contributions of the main formation (a) and loss (b) mechanisms of NO_2 as a function of N_2 content, for a residence time of 0.73 s and a SEI of approx. 12 J cm^{-3}.

As is clear from Fig. 7(b), the dominant loss mechanism of NO_2, for all N_2 fractions, is the reaction with O atoms, forming NO and O_2, which is also the most important formation mechanism of NO, see Fig. 6(a) above. Some other loss mechanisms are the formation of N_2O_3 through three-body recombination with NO, the formation of NO_3 through three-body recombination with O (and N_2 as a third body), and the formation of N_2O_5 through three-body recombination with NO_3, but they clearly play a minor role, as seen from Fig. 7(b). Note that the rates of formation of N_2O_5 (by the three-body recombination reaction between NO_2 and NO_3; the pink curve in Fig. 7(b)) and its dissociation into NO_2 and NO_3 (upon collision with a neutral particle; the blue curve in Fig. 7(a)) are almost equal to each other. This indicates that these molecules are equally converted into each other, as will also be visible from the reaction scheme in Fig. 9 below.

Finally, in Fig. 8(a) and (b) we show the main N_2O formation and loss processes, respectively. The dominant formation mechanism of N_2O is the reaction between N and NO_2, forming N_2O and O. Only at N_2 fractions below 5%, N_2O is mainly formed by the reaction between NCO and NO, forming N_2O and CO. Finally, the reaction between the metastable $N_2(A^3\Sigma_u^+)$ molecules and O_2, forming N_2O and O, also makes a minor contribution (~5–20%).

The main loss mechanism of N_2O is the reaction with $N_2(A^3\Sigma_u^+)$, forming N_2, N and NO. Only at low N_2 fractions, the charge transfer reactions with N_2^+ ions, forming either N_2O^+ and N_2, or NO^+, N and N_2, play a minor role (up to 30% at 1% N_2 fraction), while electron impact ionization also has a small, yet non-negligible contribution towards the destruction of N_2O (~5–10% at 1% N_2 fraction).

With these data, we can compose an overall reaction scheme, as presented in Fig. 9. The width of the full arrows is scaled according to the values of the time integrated reaction rates. Fig. 9(a) illustrates the main products arising from CO_2, which will subsequently react with the N-compounds presented in Fig. 9(b) and (c). Below the most important processes will be described. Initially, N_2 will be excited to its metastable state $N_2(A^3\Sigma_u^+)$, which will react with O atoms in the formation of NO, or with O_2 creating N_2O. Upon electron impact dissociation, N_2 will also be split into N atoms, which can react with both O and O_3 yielding NO. Subsequently, NO can be converted into NO_2 through a reaction with O, but NO_2 will also react back into NO upon reaction with O. This makes NO_2 the main source of NO production and *vice versa*, as is clear from Fig. 9(b). Furthermore, the N atoms, which are directly formed from N_2 dissociation, also play a role in the conversion between NO and NO_2. From NO there is also a pathway back to N_2 upon reaction with N or $N_2(a'^1\Sigma_u^-)$, and a pathway back to N upon reaction with $N_2(a'^1\Sigma_u^-)$. Furthermore, N_2O can also react back to N_2 and N upon reaction with $N_2(A^3\Sigma_u^+)$ and N_2^+. NO_2, on the other hand, has no significant

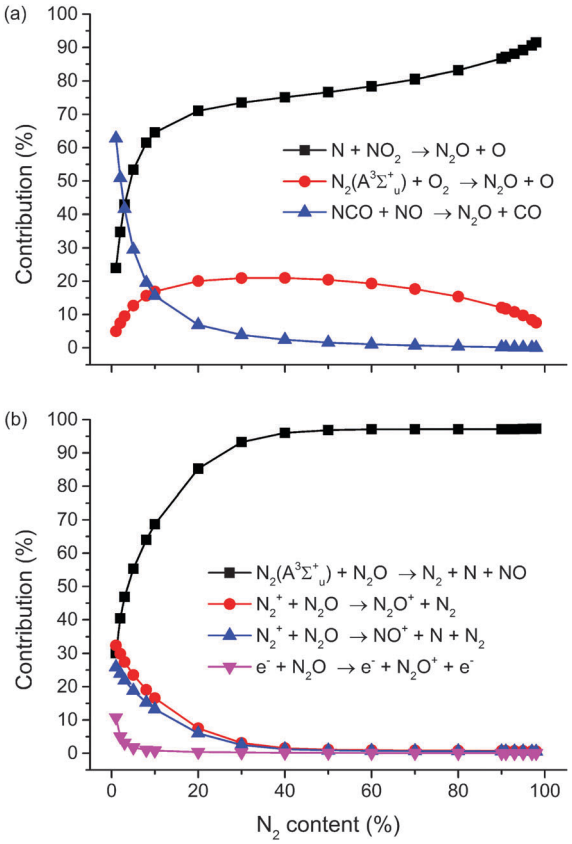

Fig. 8 Relative contributions of the main formation (a) and loss (b) mechanisms of N_2O as a function of N_2 content, for a residence time of 0.73 s and a SEI of approx. 12 J cm^{-3}.

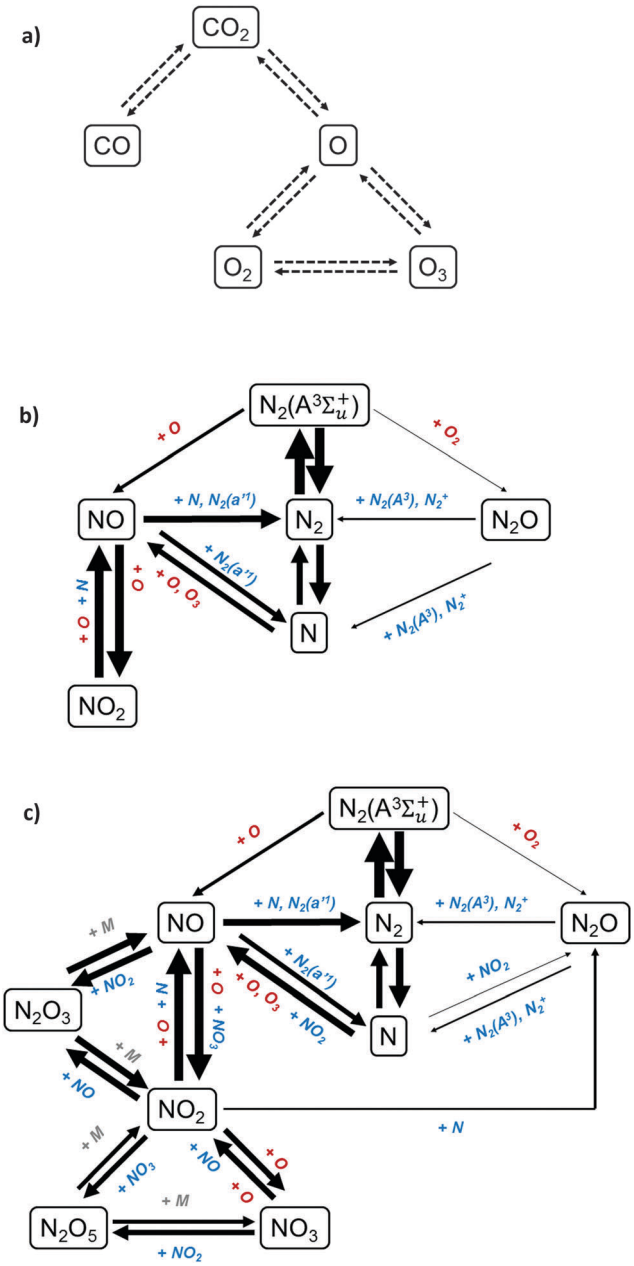

Fig. 9 Reaction scheme to illustrate the main pathways of the N_2O and NO_x chemistry as predicted by the model. Reaction pathways starting from CO_2 (a), initiation of the NO_x chemistry (b), complete overview of the N_2O and NO_x chemistry (c). The thickness of the arrows corresponds to the importance of the reactions.

pathway back to N_2 or N. This is all illustrated in Fig. 9(b), which represents the start of the different chemical pathways. This will be important to keep in mind in the further discussion below, as it will allow us to see whether we can intervene in the chemistry taking place.

Subsequently, a loop between NO, NO_2 and N_2O_3, as well as a loop between NO_2, NO_3 and N_2O_5, is created, as presented in Fig. 9(c). Furthermore, some of the NO_2 is also lost to N_2O through reaction with N radicals. The only way out of these loops, as mentioned above, is through the reaction of NO with N or $N_2(a'^1\Sigma_u^-)$, yielding either N or N_2 and an O atom, or through the reaction of N_2O with $N_2(A^3\Sigma_u^+)$ or N_2^+, leading to N_2, NO and a N atom, or to NO^+, N_2 and N or N_2O^+ and N_2, respectively.

From these reaction schemes it becomes obvious that, with respect to the plasma chemistry, there are two possibilities to prevent the formation of N_2O and NO_x compounds. The first one is to prevent the formation of the N-species involved in these reactions, *i.e.* metastable $N_2(A^3\Sigma_u^+)$ and N. This would only be possible in a plasma set-up in which all the electrons have an energy lower than 6.2 eV, which is the excitation threshold energy for the formation of $N_2(A^3\Sigma_u^+)$ through electron impact, while the dissociation threshold of N_2 into N lies at 9.75 eV. These conditions are not possible with a classic DBD. Set-ups which operate at lower average electron energies than a DBD are gliding arcs and microwave discharges. Indeed, in the model for the CO_2/N_2 microwave plasma by Heijkers *et al.*[25] it was shown that metastable $N_2(A^3\Sigma_u^+)$ is of minor importance. Nevertheless, the formation of NO_x was also observed, albeit through a different mechanism. Indeed, in a microwave plasma, the lower energy of the electrons causes vibrational excitation to become more important than electronic excitation and dissociation, and the vibrationally excited N_2 molecules react with O atoms to form N and NO, instead of the electronically excited N_2 in a DBD.

The second, more realistic option is to prevent the reaction between the N-species ($N_2(A^3\Sigma_u^+)$ and N) and the O-species

(O, O_2 or O_3), which is the initial pathway for the formation of NO and N_2O (*cf.* Fig. 9(b) above). In order to achieve this, one should look for quenching mechanisms of the $N_2(A^3\Sigma_u^+)$ metastable molecules, or possible scavengers, catalyst interactions or separation membranes for the N atoms and the O-species. Quenching of metastable molecules can be realized upon collision with other molecules. Although possible in theory, this will not be easy to realize in practice. Moreover, it is even not advisable, because exactly these metastable $N_2(A^3\Sigma_u^+)$ molecules aid in the conversion of CO_2 upon increasing N_2 content, as shown in Fig. 5. With respect to the O-species, it is important to notice that in a DBD plasma operating in CO_2 all O_2 and O_3 are originating from O (*cf.* Fig. 9(a)). Thus, when eliminating O, we automatically eliminate O_2 and O_3. Furthermore, from Fig. 9(c) it becomes clear that if we only succeed in eliminating O_2 and O_3, but not the O atoms, there is still a pathway from NO_2 to N_2O upon reaction with N atoms. This stresses the importance of trying to eliminate especially the O atoms.

In the three cases suggested above to eliminate the O-species, the main idea is the same, *i.e.*, to find an interaction which makes the O atoms or O_2 and O_3 molecules no longer available as reactants, and most importantly, this interaction has to be significantly faster than the reaction between $N_2(A^3\Sigma_u^+)$ and O or O_2; and between N and O or O_3. An example of a scavenger in the case of O is H, which reacts very fast with O to form OH and subsequently to H_2O. This effectively traps the O atoms, as was proven to be possible by a combined experimental and computational study of Aerts *et al.*[20] Another well-known scavenger of O is O_2, reacting to O_3. However, since the latter product reacts again to form O and O_2, and furthermore O_3 is also unwanted, it is not a suitable choice in this case. Furthermore, the advantage of H as a scavenger is that the scavenged product, H_2O, can be easily separated from the gas mixture. For the second option, *i.e.*, catalyst interactions, the idea of using a catalyst with a high surface interaction with O atoms, allowing the recombination reaction to O_2 on its surface,[79] is not a good choice. Indeed, in this way O_2 would be released in the plasma and it could undergo reactions again. A more advanced catalytic process that could be an option is an alternative form of chemical looping,[80,81] in which the O (or O_2) is captured in the plasma set-up and then used as an oxidizing agent in a second set-up. The third method, based on separation membrane technology, could be considered as similar to the catalyst, but instead of recombining the O to O_2 on the surface, the O atoms (or O_2 molecules) would be transported away from the reaction mixture. A last option could be the combination of a solid oxide electrolyser cell with a plasma set-up.[82] It should be realized, however, that the options mentioned above for catalysts, membranes and electrolyser cells, have only been applied up to now to separate O_2 from the gas mixture, and not the O atoms, while it is clear, as mentioned above, that in order to avoid the formation of all NO_x compounds, we need to be one step ahead and thus, we need to be able to trap already the O atoms, which is still a challenge.

If one of these concepts could be realized, it would eliminate the need for a pre-purification (N_2) or post-purification (denox) step, and thus reduce the cost of the overall process. Indeed, besides the N_2O and NO_x formation, the presence of N_2 in the gas mixture has no detrimental effect, as the effective CO_2 conversion remains more or less constant up to a N_2 fraction of 50%, as shown in Fig. 1(b), because the lower CO_2 fraction in the mixture is compensated for by the higher absolute CO_2 conversion due to the $N_2(A^3\Sigma_u^+)$ metastable molecules.

Future work should also address other impurities such as noble gases (*e.g.* He and Ar) or molecular gases such as H_2 and hydrocarbons. The presence of He and Ar should not affect the chemical pathways and products. They will mainly influence the electrical characteristics of the plasma. More specifically, their presence will lower the breakdown voltage. This was demonstrated in previous work by our own group and others.[17,83] Only for very high concentrations, the addition of noble gases would lead to a diluting effect.[84]

H_2 and hydrocarbons, on the other hand, will have an important influence on the chemical pathways and products. For example, we expect H_2 and CH_4 to have the same influence as reported in our previous work.[20] Both will be split in H atoms upon electron impact reactions, and the latter will react very fast with the O atoms present, leading to OH and subsequently to H_2O. As mentioned above, this might eliminate the production of NO_x compounds. Furthermore, this might lead to a slightly increased CO_2 conversion, since the O atoms are being directed to a liquid product.

Conclusions

The purpose of this work was to obtain a better understanding of the effect of N_2 (in the range between 1 and 98%) on the CO_2 splitting in DBD plasma, by means of an extensive combined experimental and computational study. We focused on the effect on CO_2 conversion, both absolute and effective, and the energy efficiency, as well as on the formation of N-containing byproducts, like N_2O and NO_x compounds.

We made a comparison between the measured CO_2 and N_2 conversions and the energy efficiency for CO_2 conversion, and the corresponding values calculated by means of a 0D chemical kinetics model, for the entire range of N_2 fractions. A good agreement was reached between the experimental data and the model predictions, indicating that the model includes the correct plasma chemistry and can be used to describe the main production and loss pathways for the various compounds. This allows us to gain sufficient insight into the entire process, and to propose solutions for improving the process in the future.

Our study clearly reveals that the presence of N_2 in the gas mixture up to 50% barely influences the effective CO_2 conversion and the corresponding energy efficiency, in spite of the lower CO_2 fraction in the mixture (and thus the lower CO_2 amount available for conversion). The reason is that N_2 enhances the absolute CO_2 conversion, due to the dissociation of CO_2 upon collision with $N_2(A^3\Sigma_u^+)$ metastable molecules, and both effects compensate each other. On the other hand, N_2 admixtures above 50% result in an exponential drop in the effective CO_2 conversion and energy efficiency, because more and more energy is

consumed by N_2 molecules, and not used anymore for CO_2 conversion. This means that, for mixtures containing up to 50% N_2, no pre-separation steps are necessary with respect to the effective conversion and energy efficiency.

On the other hand, the presence of N_2 in the mixture leads to the formation of N_2O and several NO_x compounds, with concentrations in the range of several 100 ppm. While these concentrations are too low to be considered useful for nitrogen fixation, they will give rise to several environmental problems. N_2O is an even more potent greenhouse gas than CO_2, with a GWP of 298 $CO_{2,equivalent}$, while NO and NO_2 are responsible for acid rain and the formation of ozone and a wide variety of toxic products. Thus, from the point of view of byproduct formation, it would be necessary to use either a pre-purification (N_2) or post-purification (denox) step.

Our detailed chemical kinetics analysis tells us that the production of these N_2O and NO_x compounds starts through a reaction between metastable $N_2(A^3\Sigma_u^+)$ molecules and either O or O_2 and between N atoms and either O or O_3; yielding the formation of NO or N_2O. Subsequently, the N is trapped in three reaction loops between the various NO_x compounds and N_2O, and the only way out is through the reaction of NO or N_2O with either N or $N_2(A^3\Sigma_u^+)$, yielding the formation of either N or N_2 and O atoms. On the plasma chemistry level, we believe that the only option to prevent the formation of N_2O and NO_x compounds is by inhibiting the reaction between the N-species ($N_2(A^3\Sigma_u^+)$ and N) and the O species (O, O_2 or O_3). To realize this, we should search for possible scavengers, catalyst interactions or separation membranes, especially for the O atoms, since this would also inhibit the formation of O_2 and O_3. If this could be successful, it would effectively eliminate the need for a pre-purification (N_2) or post-purification (denox) step.

Acknowledgements

The authors acknowledge financial support from the IAP/7 (Inter-university Attraction Pole) program 'PSI-Physical Chemistry of Plasma-Surface Interactions', financially supported by the Belgian Federal Office for Science Policy (BELSPO), as well as the Fund for Scientific Research Flanders (FWO). This work was carried out in part using the Turing HPC infrastructure at the CalcUA core facility of the Universiteit Antwerpen, a division of the Flemish Supercomputer Center VSC, funded by the Hercules Foundation, the Flemish Government (department EWI) and the University of Antwerp.

Notes and references

1 L. Johnson, J. Grant and P. L. Low, *Two degrees of separation: ambition and reality: low Carbon Economy Index 2014*, 2014.
2 C. B. Field, V. R. Barros, D. J. Dokken, K. J. Mach, M. D. Mastrandrea, T. E. Bilir, M. Chatterjee, K. L. Ebi, Y. O. Estrada, R. C. Genova, B. Girma, E. S. Kissel, A. N. Levy, S. MacCracken, P. R. Mastrandrea and L. L. White, *IPCC, 2014: Climate Change 2014 Impacts, Adaptation, and Vulnerability. Part A: Global and Sectoral Aspects. Contribution of Working Group II to the Fifth Assessment Report of the Intergovernmental Panel on Climate Change*, Cambridge University Press, 2014.
3 C. Lagarde, Int. Monet. Fund.
4 G. Nichols Roth, *G7 Climate Change The New Economy*, World News-Climate Change The New Economy Ltd, 2015.
5 G. Centi, E. A. Quadrelli and S. Perathoner, *Energy Environ. Sci.*, 2013, **6**, 1711–1731.
6 G. Centi and S. Perathoner, *Catal. Today*, 2009, **148**, 191–205.
7 W. McDonough, M. Braungart, P. Anastas and J. Zimmerman, *Environ. Sci. Technol.*, 2003, **37**, 434A–441A.
8 E. E. Benson, C. P. Kubiak, A. J. Sathrum and J. M. Smieja, *Chem. Soc. Rev.*, 2009, **38**, 89–99.
9 M. Aresta, A. Dibenedetto and A. Angelini, *Chem. Rev.*, 2014, **114**, 1709–1742.
10 J. R. Scheffe and A. Steinfeld, *Mater. Today*, 2014, 1–8.
11 E. V. Kondratenko, G. Mul, J. Baltrusaitis, G. O. Larrazábal and J. Pérez-Ramírez, *Energy Environ. Sci.*, 2013, **6**, 3112.
12 A. Goeppert, M. Czaun, J.-P. Jones, G. K. Surya Prakash and G. a. Olah, *Chem. Soc. Rev.*, 2014, **43**, 7995–8048.
13 A. H. McDaniel, E. C. Miller, D. Arifin, A. Ambrosini, E. N. Coker, R. O'Hayre, W. C. Chueh and J. Tong, *Energy Environ. Sci.*, 2013, **6**, 2424.
14 E. N. Coker, A. Ambrosini, M. a. Rodriguez and J. E. Miller, *J. Mater. Chem.*, 2011, **21**, 10767.
15 S. Samukawa, M. Hori, S. Rauf, K. Tachibana, P. Bruggeman, G. Kroesen, J. C. Whitehead, A. B. Murphy, A. F. Gutsol, S. Starikovskaia, U. Kortshagen, J.-P. Boeuf, T. J. Sommerer, M. J. Kushner, U. Czarnetzki and N. Mason, *J. Phys. D: Appl. Phys.*, 2012, **45**, 253001.
16 R. Aerts, W. Somers and A. Bogaerts, *ChemSusChem*, 2015, **8**, 702–716.
17 M. Ramakers, I. Michielsen, R. Aerts, V. Meynen and A. Bogaerts, *Plasma Processes Polym.*, 2015, **12**, 755–763.
18 R. Aerts, T. Martens and A. Bogaerts, *J. Phys. Chem. C*, 2012, **116**, 23257–23273.
19 F. Brehmer, S. Welzel, R. M. C. M. Van De Sanden and R. Engeln, *J. Appl. Phys.*, 2014, **116**, 123303.
20 R. Aerts, R. Snoeckx and A. Bogaerts, *Plasma Processes Polym.*, 2014, **11**, 985–992.
21 K. Van Laer and A. Bogaerts, *Energy Technol.*, 2015, **3**, 1038–1044.
22 T. Kozák and A. Bogaerts, *Plasma Sources Sci. Technol.*, 2014, **23**, 045004.
23 A. P. H. Goede, W. A. Bongers, M. F. Graswinckel, R. M. C. M. Van De Sanden, M. Leins, J. Kopecki, A. Schulz and M. Walker, *EPJ Web Conf.*, 2014, **79**, 01005.
24 T. Silva, N. Britun, T. Godfroid and R. Snyders, *Plasma Sources Sci. Technol.*, 2014, **23**, 025009.
25 S. Heijkers, R. Snoeckx, T. Kozák, T. Silva, T. Godfroid, N. Britun, R. Snyders and A. Bogaerts, *J. Phys. Chem. C*, 2015, **119**, 12815–12828.

26 L. F. Spencer and A. D. Gallimore, *Plasma Sources Sci. Technol.*, 2013, **22**, 015019.
27 A. Indarto, J.-W. Choi, H. Lee and H. K. Song, *Environ. Eng. Sci.*, 2006, **23**, 1033–1043.
28 A. Indarto, D. R. Yang, J.-W. Choi, H. Lee and H. K. Song, *J. Hazard. Mater.*, 2007, **146**, 309–315.
29 T. Nunnally, K. Gutsol, A. Rabinovich, A. Fridman, A. Gutsol and A. Kemoun, *J. Phys. D: Appl. Phys.*, 2011, **44**, 274009.
30 X. Tao, M. Bai, X. Li, H. Long, S. Shang, Y. Yin and X. Dai, *Prog. Energy Combust. Sci.*, 2011, **37**, 113–124.
31 G. Petitpas, J. Rollier, A. Darmon, J. Gonzalez-Aguilar, R. Metkemeijer and L. Fulcheri, *Int. J. Hydrogen Energy*, 2007, **32**, 2848–2867.
32 C. Liu, G. Xu and T. Wang, *Fuel Process. Technol.*, 1999, **58**, 119–134.
33 R. Snoeckx, Y. X. Zeng, X. Tu and A. Bogaerts, *RSC Adv.*, 2015, **5**, 29799–29808.
34 A. Janeco, N. R. Pinha and V. Guerra, *J. Phys. Chem. C*, 2015, **119**, 109–120.
35 R. Snoeckx, R. Aerts, X. Tu and A. Bogaerts, *J. Phys. Chem. C*, 2013, **117**, 4957–4970.
36 G. Scarduelli, G. Guella, D. Ascenzi and P. Tosi, *Plasma Processes Polym.*, 2011, **8**, 25–31.
37 Y. Zhang, Y. Li, Y. Wang, C. Liu and B. Eliasson, *Fuel Process. Technol.*, 2003, **83**, 101–109.
38 X. Zhang and M. S. Cha, *J. Phys. D: Appl. Phys.*, 2013, **46**, 415205.
39 L. M. Martini, G. Dilecce, G. Guella, A. Maranzana, G. Tonachini and P. Tosi, *Chem. Phys. Lett.*, 2014, **593**, 55–60.
40 D. Li, X. Li, M. Bai, X. Tao, S. Shang, X. Dai and Y. Yin, *Int. J. Hydrogen Energy*, 2009, **34**, 308–313.
41 X. Tu, H. J. Gallon, M. V. Twigg, P. a. Gorry and J. C. Whitehead, *J. Phys. D: Appl. Phys.*, 2011, **44**, 274007.
42 B. Eliasson, C. Liu and U. Kogelschatz, *Ind. Eng. Chem. Res.*, 2000, **39**, 1221–1227.
43 V. J. Rico, J. L. Hueso, J. Cotrino and A. R. González-Elipe, *J. Phys. Chem. A*, 2010, **114**, 4009–4016.
44 X. Tu and J. C. Whitehead, *Appl. Catal., B*, 2012, **125**, 439–448.
45 Q. Wang, Y. Cheng and Y. Jin, *Catal. Today*, 2009, **148**, 275–282.
46 B. Fidalgo, A. Domínguez, J. Pis and J. Menéndez, *Int. J. Hydrogen Energy*, 2008, **33**, 4337–4344.
47 A. Indarto, J. Choi, H. Lee and H. Song, *Energy*, 2006, **31**, 2986–2995.
48 B. Eliasson, U. Kogelschatz, B. Xue and L.-M. Zhou, *Ind. Eng. Chem. Res.*, 1998, **37**, 3350–3357.
49 M. Kano, G. Satoh and S. Iizuka, *Plasma Chem. Plasma Process.*, 2011, **32**, 177–185.
50 S. Futamura and H. Kabashima, *Stud. Surf. Sci. Catal.*, 2004, **153**, 119–124.
51 T. Ihara, M. Kiboku and Y. Iriyama, *Bull. Chem. Soc. Jpn.*, 1994, **67**, 312–314.
52 T. Ihara, T. Ouro, T. Ochiai, M. Kiboku and Y. Iriyama, *Bull. Chem. Soc. Jpn.*, 1996, **69**, 241–244.
53 G. Chen, T. Silva, V. Georgieva, T. Godfroid, N. Britun, R. Snyders and M. P. Delplancke-Ogletree, *Int. J. Hydrogen Energy*, 2015, **40**, 3789–3796.
54 A. Gutsol, A. Rabinovich and A. Fridman, *J. Phys. D: Appl. Phys.*, 2011, **44**, 274001.
55 E. C. Neyts and a. Bogaerts, *J. Phys. D: Appl. Phys.*, 2014, **47**, 224010.
56 T. Nozaki and K. Okazaki, *Catal. Today*, 2013, **211**, 29–38.
57 V. J. Rico, J. Cotrino, R. Gonza and R. M. Lambert, *ACS Catal.*, 2014, **4**, 402–408.
58 A. Fridman, *Plasma chemistry*, Cambridge University Press, New York, 2008.
59 H. L. Chen, H. M. Lee, S. H. Chen and M. B. Chang, *Ind. Eng. Chem. Res.*, 2008, **47**, 2122–2130.
60 B. S. Patil, Q. Wang, V. Hessel and J. Lang, *Catal. Today*, 2015, **256**, 49–66.
61 N. R. Pinhão, A. Moura, J. B. Branco and J. Neves, *Int. J. Hydrogen Energy*, 2015, submitted.
62 S. Pancheshnyi, B. Eismann, G. J. M. Hagelaar and L. C. Pitchford, Computer code ZDPlasKin, University of Toulouse, LAPLACE, CNRS-UPS-INP, Toulouse, France, 2008, http://www.zdplaskin.laplace.univ-tlse.fr.
63 G. J. M. Hagelaar and L. C. Pitchford, *Plasma Sources Sci. Technol.*, 2005, **14**, 722–733.
64 U. Kogelschatz, *Plasma Chem. Plasma Process.*, 2003, **23**, 1–46.
65 R. Snoeckx, M. Setareh, R. Aerts, P. Simon, A. Maghari and A. Bogaerts, *Int. J. Hydrogen Energy*, 2013, **38**, 16098–16120.
66 R. Aerts, X. Tu, W. Van Gaens, J. C. Whitehead and A. Bogaerts, *Environ. Sci. Technol.*, 2013, **47**, 6478–6485.
67 A. Majumdar, J. F. Behnke, R. Hippler, K. Matyash and R. Schneider, *J. Phys. Chem. A*, 2005, **109**, 9371–9377.
68 *Convention on Long-Range Transboundary Air Pollution*, 1979, http://www.unece.org/fileadmin/DAM/env/lrtap/full%20text/1979.CLRTAP.e.pdf.
69 N. Fontaine and A. Neyts-Uytterbroeck, *Off. J. Eur. Communities*, 2001, **309**, 22–30.
70 T. J. Pilusa, *Aerosol Air Qual. Res.*, 2012, 994–1006.
71 H.-G. Pöttering and G. Gloser, *Off. J. Eur. Communities*, 2007, **171**, 1–16.
72 Integrated Pollution Prevention and Control: Reference Document on Best Available Techniques for Large Combustion Plants, European Commision, 2006.
73 C. Baird and M. Cann, *Environmental Chemistry*, W. H. Freeman and company, New York, 4th edn, 2008.
74 V. Smil, *Enriching the earth: Fritz Haber, Carl Bosch, and the transformation of world food production*, MIT Press, 2004.
75 R. Atkinson, D. L. Baulch, R. a. Cox, J. N. Crowley, R. F. Hampson, R. G. Hynes, M. E. Jenkin, M. J. Rossi and J. Troe, *Atmos. Chem. Phys. Discuss.*, 2003, **3**, 6179–6699.
76 K. Skalska, J. S. Miller and S. Ledakowicz, *Sci. Total Environ.*, 2010, **408**, 3976–3989.
77 S. Roy, M. S. Hegde and G. Madras, *Appl. Energy*, 2009, **86**, 2283–2297.
78 W. Van Gaens and A. Bogaerts, *Plasma Sources Sci. Technol.*, 2014, **23**, 035015.

79 Y. C. Kim and M. Boudart, *Langmuir*, 1991, **7**, 2999–3005.
80 J. Adanez, A. Abad, F. Garcia-Labiano, P. Gayan and L. F. de Diego, *Prog. Energy Combust. Sci.*, 2012, **38**, 215–282.
81 M. M. Hossain and H. I. de Lasa, *Chem. Eng. Sci.*, 2008, **63**, 4433–4451.
82 Y. Tagawa, S. Mori, M. Suzuki, I. Yamanaka, T. Obara, J. Ryu and Y. Kato, *Kagaku Kogaku Ronbunshu*, 2011, **37**, 114–119.
83 N. R. Pinhão, A. Janeco and J. B. Branco, *Plasma Chem. Plasma Process.*, 2011, **31**, 427–439.
84 V. Goujard, J.-M. Tatibouët and C. Batiot-Dupeyrat, *Plasma Chem. Plasma Process.*, 2011, **31**, 315–325.